Progress in Oceanography 237 (2025) 103512

Contents lists available at ScienceDirect

Progress in Oceanography

journal homepage: www.elsevier.com/locate/pocean

Does the oceanographic response to wind farm wind-wakes affect the spring phytoplankton bloom?

Arianna Zampollo [a,*], Rory O'Hara Murray [b], Alejandro Gallego [b], Beth Scott [a]

[a] University of Aberdeen, Zoology Building, Tillydrone Ave, Aberdeen, United Kingdom AB24 2TZ
[b] Marine Directorate of the Scottish Government, 375 Victoria Rd, Aberdeen, United Kingdom AB11 9DB

ARTICLE INFO

Keywords:
Chlorophyll
Wind Speed Reduction
Ocean Model
Dipoles
Water Stratification
Hydrodynamic Change
North-West North Sea

ABSTRACT

Large offshore wind farms (OWFs) will be deployed in the North Sea, potentially causing multiple effects on marine ecosystems some of which may be synergistic with climate change. This study modelled the oceanographic bio-physical response to anticipated atmospheric wind farm wakes in the north-west North Sea. The wind wake was included as a reduction of the wind speed into the atmospheric forcing of the Finite Volume Community Ocean Model (FVCOM) coupled with the European Regional Sea Model (ERSEM) from three OWFs using a year with available *in situ* data for model validation. The spatial distribution of physical variables and chlorophyll *a* (Chl-a) was compared between model runs with and without OWFs during three temporal subdivisions (pre-bloom, bloom and post-bloom) of the spring-summer period. Overall, across the entire period there was a 7 % decrease in Chl-a concentration, with the decrease being more pronounced during the bloom period. However, there was a slight increase in Chl-a in the post-bloom period. At higher temporal (12 h) and spatial (> 1 km) scales, significant changes in Chl-a were identified throughout the vertical water column and during the prevailing south-west and north-west winds, which generated a persistent upwelling/downwelling dipole across the simulated time series. The spatial variations of potential energy anomaly (PEA) and Chl-a were the most informative variables as they displayed distinct values and spatial distributions linked to the upwelling/downwelling dipoles. The downwelling cell was characterised by fresher and warmer waters, especially at the surface, with areas displaying an increase in stratification with a resulting decrease of Chl-a in seasonally stratified waters. On the other hand, upwelling regions were characterised by saltier and cooler waters with increasing PEA in permanently mixed and intermittently stratified waters showing consistently increased Chl-a production. The changes to levels of stratification are ecologically important as they change the vertical characteristics of the water column differently over a seasonal cycle. The analyses confirmed that it is critical to identify the temporal and spatial scales at which important changes to the physics and Chl-a production occur as they will play a role in assessing the range of impacts of OWFs.

1. Introduction

The increasing urgency of reducing carbon dioxide emissions has led North Sea countries to develop spatial and sector planning policies supporting the installation of offshore renewable energy facilities. At least 260 GW of offshore wind farms (OWFs), with a further 75 GW in the UK alone, are planned to be deployed in the North Sea by 2050 (Draft Energy Strategy and Just Transition Plan, 2023) with the complex effects on marine ecosystems still mostly unknown. To date, cumulative impact assessments are addressed by several European directives (Directive 2001/42/EC, Directive 2008/56/EC, Directive 2014/42/EC) although clear guidelines on the protection of whole marine ecosystems (rather than individual species) have not yet been delineated for licensing, environmental impact assessment and post-consent measures (Declerck et al., 2023).

Wind turbines are deployed on different types of foundations (e.g. monopile, jacket, or floating), which act as a barrier in the water column and can impact the surrounding hydrodynamic conditions (Dorrell et al., 2022; Floeter et al., 2017). Wind turbines not only potentially alter the mixing budget of the water column through their foundations (monopiles – Floeter et al., 2017, or floating – Dorrell et al., 2022), they also influence the atmospheric conditions above the sea surface by converting wind kinetic energy into mechanical energy to generate

* Corresponding author.
E-mail addresses: zampolloarianna@gmail.com (A. Zampollo), rory.murray@gov.scot (R.O. Murray), alejandro.gallego@gov.scot (A. Gallego), b.e.scott@abdn.ac.uk (B. Scott).

https://doi.org/10.1016/j.pocean.2025.103512
Received 13 September 2024; Received in revised form 22 April 2025; Accepted 28 May 2025
Available online 30 May 2025

Abbreviations

Chl-a	chlorophyll-a
$\int$Chl-a	depth-integrated Chl-a throughout the water column, $\int_{z_0}^{z_b} Chla(z)\,dx$, where z_0 is the sea surface, z_b is the seabed
$Chla_{tot}$	total amount of Chl-a over time and across the domain
ICOL	Inch Cape Offshore Wind Limited
M_B	baseline model
M_{WF}	wind farm model
SCML	subsurface chlorophyll maximum layer
MSFD	Marine Strategy Framework Directive
NCMPA	Nature Conservation Marine Protected Areas
NnG	Neart na Gaoithe Offshore Wind Limited
OWF	offshore wind farm
PEA	potential energy anomaly
S	salinity
SSH	sea surface height
SWEL	Seagreen Wind Energy Limited
T	temperature
u	horizontal current

electricity (Ali et al., 2023). One of the most documented changes is the creation of atmospheric wakes (Emeis, 2010), a region where the downstream flow of air is disrupted, wind speed changed and turbulence increased (Ali et al., 2023). This can result in localised changes in temperature and humidity, which can further influence weather patterns and marine environments. The wind wake is an area downstream of OWFs where the wind speed above the surface can be reduced up to 40 % close to the farm site and recover up to 70 km downwind in stable atmospheric conditions (Platis et al., 2018). The modelled scenarios of reduced wind speed along a wind wake reported changes in the sea surface temperature and vertical movements throughout the water column (Ludewig, 2015). The reduced Ekman transport resulting from the wind wake region modifies the vertical and horizontal movement of water near the wind farms, generating two regions, one of surface water converging, evolving into downwelling of relatively less dense (warm/fresh) water, and one of surface water diverging and replaced by upward fluxes of relatively dense (cold/salty) waters (Ludewig, 2015). This formation of an upwelling and downwelling dipole influences the temperature, salinity, water elevation, mixing and stratification balances in these regions. Upward and downward fluxes changed the surface mixed layer depth (Christiansen et al., 2022a; Daewel et al., 2022), hence altering the structure of stratified water columns (Floeter et al., 2022). Daewel et al. (2022) reported a distribution of negative and positive changes in annual net primary production in the North Sea associated with variations in the stratification of the water column, advocating that the upwelling and downwelling patterns play a major role in changing marine ecosystems (Floeter et al., 2017, 2022). The response of each region to the reduction or enhancement of mixing/stratification will also depend on the hydrodynamic conditions supporting the regional ecosystem. Hence, the distribution, distance and magnitude at which OWF-induced changes occur might depend on different factors: i) the direct action of the turbines' foundations on the hydrodynamics (increasing turbulence downstream the foundations, Carpenter et al., 2016) and the reduced wind stress downstream the turbine rotors (Ludewig, 2015), and ii) the resonance of the physical changes on the primary production within hydrodynamic regimes (van Leeuwen et al., 2015), which are driving whole ecosystem interactions via bottom-up regulation by hydrodynamic processes (Trifonova et al., 2021). For example, reduced primary production in the southern North Sea appeared at known productive fronts (Daewel et al., 2022), while increased stratification over typically dynamic waters nearshore, such as the German Bight and Dogger Bank, exhibited increasing net primary production (van der Molen et al., 2014).

Although the OWF-induced effects on the atmospheric conditions will involve more than just a reduction in wind speed (e.g. increasing turbulence and wind speed at specific locations), this research explored the potential impacts of wind speed reduction within OWF wind wakes on the physics and phytoplankton production of a seasonally stratified shelf sea. Oceanographic conditions were compared between modelled scenarios with and without three wind farms consented in the Firth of Forth and Firth of Tay region (Scotland, UK). Only the reduced wind speed within the farm and the wake lee were used to represent the effect of OWFs in the modelled wind farm scenario. Variations in abiotic factors and chlorophyll-a (Chl-a) concentration were examined across fine and larger temporal and spatial scales before, throughout, and after the spring phytoplankton bloom, utilising a significant number of *in situ* observations collected in 2003 to validate the baseline model (without wind farms).

2. Method

2.1. Study area

The effects of the wind energy extraction on shelf seas were investigated in the north-west section of the North Sea, in the Scottish waters off Edinburgh (UK) (Fig. 1). The area hosts multiple hydrodynamic regimes defined by tidal cycles, river outflows, and a composite bathymetry characterised by localised banks (van Leeuwen et al., 2015). The Firth of Forth and Tay region is subject to spatial patchiness in chlorophyll-a (Chl-a) (used as a proxy of phytoplankton presence), being highly influenced by the spring-neap tidal cycle over submarine banks (Cox et al., 2018), near which seabirds and top predators are found to forage during relatively oligotrophic summer conditions (Scott et al., 2010). In this study, we modelled three offshore wind farms (OWFs) that are currently being deployed in waters 40–60 m above the lowest astronomical tide: Inch Cape Offshore Wind Limited (ICOL) (under development), Neart na Gaoithe Offshore Wind Limited (NnG) (under construction), and Seagreen Wind Energy Limited (SWEL) (fully operational since 2023). The location of Seagreen OWF is within three Nature Conservation Marine Protected Areas (NCMPAs, Marine (Scotland) Act, 2010) (Fig. 1) designated to protect the ocean quoahog aggregations (*Arctica islandica*), shelf banks formed during the last Ice Age, and offshore sand and gravels supporting sandeels, flatfish, starfish and crabs. The three NCMPAs overlap over regions exhibiting large stock of sandeels that sustain the seabird colonies breeding on the coastline (Wanless, 1998). A Special Area of Conservation (Directive 92/43/EEC) was designated in 2005 in the Firth of Tay and Eden Estuary due to the presence of breeding and haulout sites for harbour seals (*Phoca vitulina*). The same region is also identified as an area consistently visited by bottlenose dolphins (*Tursiops truncates*) (Arso Civil et al., 2019). Moreover, this region includes the Isle of May, which is part of the Forth Islands SPA (Directive 2009/147/EC), located about 40 km east of the Firth of Forth, where large colonies of seabirds and seals spend their breeding season during spring and summer, feeding upon productive offshore waters (Carter et al., 2022; Harris et al., 2012; Wanless, 1998). Moreover, the Outer Forth and St Andrews Bay SPA hosts seabirds during the breeding and non-breeding seasons.

2.2. Model setup and validation

The physical and biogeochemical aspects of the marine environment in the Firth of Forth and Tay region were modelled using an implementation of the Finite Volume Community Ocean Model (FVCOM) (Chen et al., 2003) for the Firth of Forth region (O'Hara Murray, 2017) coupled with the European Regional Sea Model (ERSEM) (Butenschön et al., 2016). Two scenarios, a reference baseline model (M_B) and a model containing the effect of atmospheric wind energy extraction

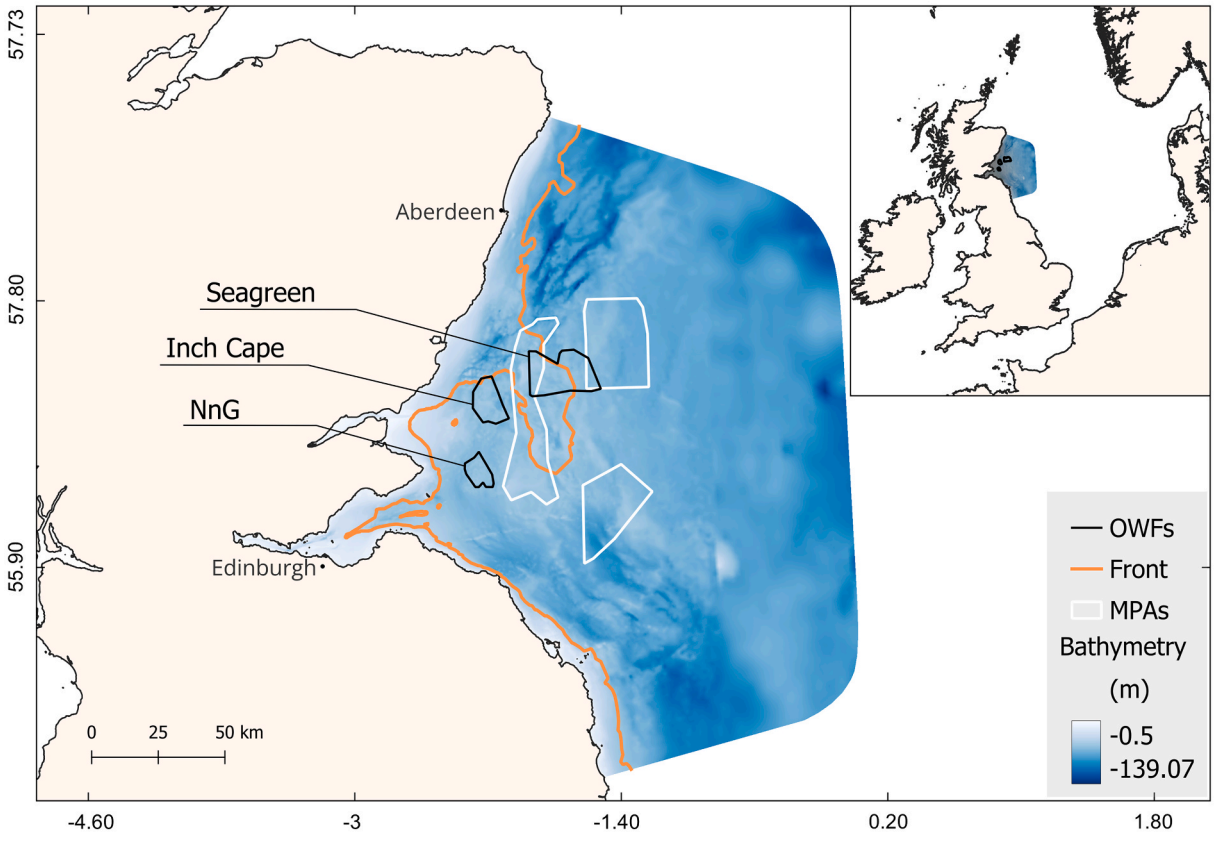

Fig. 1. Map showing the model domain of the Firth of Forth and Tay region, bathymetry (blue), offshore wind farms (OWFs, black polygons), Nature Conservation Marine Protected Areas (white polygons), and the frontal region (orange contour is potential energy anomaly below 25 J m^{-3}) where the transition between vertically mixed and stratified waters occurred during May. (For interpretation of the references to colour in this figure legend, the reader is referred to the web version of this article.)

(M_{WF}) represented as wind speed reduction within the farm wind wake (see section 2.3, Christiansen et al., 2022a), were compared to understand the effects of wind farms on the physical and biogeochemical processes before, during and after the phytoplankton bloom period in 2003 (defined using Rodionov (2004), see section 2.4.1). The model used an unstructured triangular grid with mesh sizes having nodes spacing from 70 m near the coastline to 4000 m at the eastern open boundary (Fig. 1). The vertical dimension was structured by stacking the horizontal mesh over 10 layers from the sea surface to the seabed. The thickness of these layers varied across the model domain with each layer representing 10 % of the water column (sigma co-ordinate systems). The bathymetry data were obtained from multiple sources: high resolution multibeam data from UK hydrographic office (UKHO) through the Civil Hydrography Programme and a gridded dataset from Seazone for offshore areas, interpolated to the model grid.

The physical parameters at the open boundary were forced by the outputs of the Scottish Shelf Water Reanalysis Service v. 3.02 (Barton et al., 2022), a downstream service of the Copernicus Marine Service. Hourly temperature, salinity, water elevation and velocity data were interpolated at the open boundary. Atmospheric forcing was included by interpolating hourly wind velocity, air pressure, heating fluxes and precipitations from ECMWF Reanalysis 5th Generation (ERA5) (Hersbach et al., 2023) to the mesh. Discharges (volume flux) from 12 rivers were downloaded from the National River Flow Archive (NRFA) and used in the model assuming a uniform vertical outflow.

ERSEM initial and boundary conditions for 60 biogeochemical parameters were derived from a pre-existing ERSEM simulation of the North-West European Shelf Seas (AMM7), in which ERSEM was coupled to Nucleus for European Modelling of the Ocean (NEMO) at 7 km horizontal resolution (Edwards et al., 2012). The 60 biogeochemical parameters were from 8 functional groups: bacteria, nutrients, dissolved organic matter, particulate organic matter, phytoplankton, zooplankton, heterorophic grazers and benthos. The output from this simulation was used to initialise our model and define its open boundary conditions. Following a two-month spin-up period (January and February), hourly outputs were recorded for the baseline model (M_B) and wind farm model (M_{WF}) scenarios from March and June.

2.2.1. *Validation of M_B*

The baseline model (M_B) was validated using 1,169 *in situ* profiles collected by the Marine Directorate for the Scottish Government on board the MRV *Scotia* and during the EU IMPRESS project (more details on the methods in Scott et al., 2010). Data were distributed between April and July 2003 in the Firth of Forth and Tay region (Fig. A.1 in the Appendix). The profiles of temperature, conductivity, and Chl-a were collected using a CTD equipped with a fluorometer. The values from M_B of temperature (°C), salinity (g m^{-3}) and Chl-a (mg m^{-3}) (the sum of diatom, nano-, pico- and micro-phytoplankton Chl-a output from ERSEM) were compared to the spatial and temporal closest *in situ* values. The baseline model was validated with *in situ* profiles within a maximum spatial window of $< 1{,}200$ m and a maximum temporal window of < 30 min between pairs of observations and model outputs. The comparison was performed for vertically resolved values throughout the water column and depth-integrated medians. The comparison is made using Taylor diagrams (Taylor, 2001) using R. Results and details on model validation are reported in the Appendix.

2.3. *Wind deficit parametrisation*

The offshore wind farms were included into the M_{WF} by reducing the

wind speed at 10 m above the sea surface (wind deficit Δu) over the area affected by offshore wind farms and their wakes (downstream region with reduced wind speed) (Fig. 2). The magnitude and size of the wake is typically defined by the stability of the atmospheric conditions and the types of turbines. Different lengths and deficits for OWFs are reported in Table A.1 in the Appendix.

A fixed length of the wake (σ) was set at 30 km, and a maximum relative deficit (a) of surface wind speed of 10 % was applied to each single farm. The length and deficit were selected by averaging the values reported in the literature (Table A.1), whose case studies reported similar turbine generating capacity of *circa* 10 MW to those in the Firth of Forth and Tay region. A maximum deficit of 10 % was applied homogeneously over the area occupied by the three offshore wind farms (Fig. 2). The final wind deficit was obtained by cumulating the relative deficits from the three OWFs and their wakes over overlapping areas (Fig. 2). The parametrisation of the wake effect was limited to wind speeds ranging between 3–25 m s^{-1} to reflect the cut-in and cut-out speeds of operational turbines (Akhtar et al., 2021; Christiansen et al., 2022a).

The velocity deficit Δu was parametrised from three wind farms. The change in wind speed is based on the method described by Christiansen et al. (2022a), where the deficit is given in a reference coordinate system, $\Delta u(x, y)$, where x is the distance along the wake from the wind farm aligned with the wind direction, and y is the distance from the central wake axis (Fig. 2). Christiansen et al. (2022a) defined the wind wake recovery on the x axis using an exponential decay equation from the wind farm to the furthest edge of the wake (Eq. A1) and the y axis, the wake cross-section, as half of a Gaussian distribution (Eq. A2). Hence, x and y described the distribution of the deficit in relation to the wind recovery across and along the wake.

2.4. Comparing M_B to M_{WF}

2.4.1. Temporal comparison based on periods of Chl-a productivity

Temperate seas typically experience a significant increase in phytoplankton abundance during spring, whose maximum values oscillate between March and May in the northern North Sea. The timing of the bloom is essential for top predators, particularly migratory species such as seabirds and fish, whose breeding success is partly dependent on the oscillation of the bloom period (Platt et al., 2003; Scott et al., 2006; Vikebø et al., 2012), which regulates the distribution and growth of their prey. In this study, the period exhibiting a consistent increase in Chl-a concentration ("bloom") was distinguished from the preceding ("pre-bloom") and following ("post-bloom") periods. These three periods were classified using the STARS (Sequential *T*-test Analysis of Regime Shifts) algorithm, which is designated to detect regime shifts in ecosystems undergoing persistent changes (Rodionov, 2004). STARS was selected to identify the onset and duration of the spring bloom using a sequential data processing technique to test if the daily Chl-a production over the study area is part of the current investigated regime (either pre-bloom, bloom or post-bloom), or if it is a shift point between one regime and the other (Room et al., 2022). Each observation in the current regime is compared against every new entry, and those points that significantly deviate from the current regime's average are tested as shift points between two regimes by Student's *t*-test. The algorithm was performed on daily Chl-a productions across the whole domain, and it requires two parameters, the cut-off regime length (l) and probability level (p), to draw the sequential analysis. The cut-off length is the hypothetical minimum length of regimes, and a value of $l = 10$ was selected among different values between 5 and 20 based on literature (Friedland et al., 2018). The probability level was set at 0.05 as a threshold of statistical significance that a positive result is a random event (Room et al., 2022). The analysis was run using the package *rshift* (Room et al. 2022) in R. The total amount of Chl-a across the domain was measured as:

$$Chla_{tot} = \frac{1}{n}\int_{t_1}^{t_n}\iiint_{V} Chla(x, y, z, t)dVdt \times 100$$

being t_s to t_e the hourly model outputs from start (s) to the end (e) of any timeframe (e.g. a day or the pre-bloom period) in the three-dimensional model domain ($V = x, y, z$). $Chla_{tot}$ was compared across phenological periods.

2.4.2. Spatial comparison of M_B to M_{WF}

The baseline (M_B) and wind farm (M_{WF}) models were compared over space and time. The difference in biotic and abiotic variables from the models ($\Delta = M_{WF} - M_B$) were estimated at each time step (hourly data) for each unit of the mesh. The changes (Δ) were averaged during three different phenological periods (pre-bloom, bloom and post-bloom) and over different spatial scales to evaluate how scales influence summary outcomes. The spatial correlations among Δ for potential energy anomaly (PEA), sea surface height (SSH), depth-averaged temperature

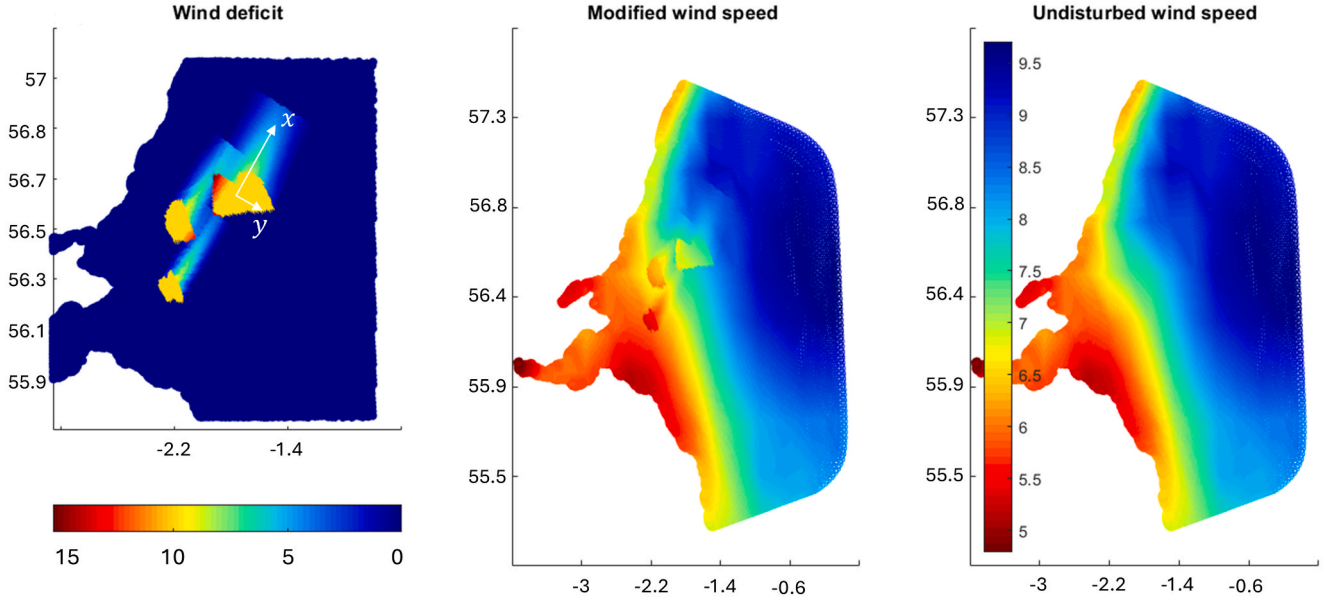

Fig. 2. (a) Map showing the wind deficit (%) where $\Delta u(x, y)$ (white arrows) is calculated for south-west wind. Maps of the wind field (m s^{-1}) in (b) M_{WF} and (c) M_B.

(T), depth-averaged salinity (S), and Chl-a were obtained using Pearson correlation coefficient (ρ) (Benesty et al., 2009) in R. Pearson's ρ and its associated statistical significance (p-value < 0.01) were used as a measure of spatial linear correlation between the values from M_B and M_{WF} at each unit of the mesh.

2.4.3. Transects of the water column during two prevailing wind directions

Two time periods, with prevailing south-west and north-west winds, were selected from the model to investigate vertical and horizontal distribution of dipoles, Chl-a and stratification. Because dipoles develop when wind direction is stable over at least 8–10 h and speeds between 5–10 m s^{-1} (Floeter et al., 2022; Ludewig, 2015), six intervals following the establishment of stable wind direction for at least 12 h were compared to determine the optimal temporal scale for assessing OWF effects, with a focus on representing the results through the averaging of physical and biological changes. The changes were examined during the post-bloom period, when food resources in summer-stratified waters affect the upper trophic layer, including fish growth (Bergstad et al., 2002) and seabirds energetics (Dunn et al., 2023). Changes were examined over a range of hydrodynamic regimes (van Leeuwen et al., 2015) defined from March to June along the transect. Waters were considered stratified when PEA > 25 J m^{-3}. Permanently mixed waters reported mixed water columns for the entire time series. Intermittently stratified waters exhibited mixed conditions for at least 2.5 days every week, while seasonally stratified waters showed mixed conditions at least every 45 days. Regions of freshwater influence (ROFI) and permanently stratified were not identified along the transect.

3. Results and Discussion

The model reported similar values to *in situ* observations throughout the vertical column for salinity, temperature and Chl-a (Fig. A4 and A5 in the Appendix). The comparison of the baseline model (M_B) to the wind farms model (M_{WF}) detailed changes of the physics and Chl-a overtime (Section 3.1). Changes occurred in coastal and offshore waters up to hundreds of kilometres away from wind farms, detailing specific patterns across spatial and temporal scales. Dipoles for upwelling and downwelling processes were identified during the three bloom phases (section 3.2) and under prevailing wind conditions (section 3.3). Opposite increases and decreases in temperature and salinity at dipoles affected PEA, which resulted in changing Chl-a concentrations in these waters.

3.1. Overall temporal variation

In this region, the pre-bloom phase occurred between 1st and 25th March (25 days), the bloom period started on 26th March and ended on 26th April (31 days), and the post-bloom started on 27th April and persisted until the end of the simulation (30th June) (65 days). At the current temporal and spatial resolution, no changes were recorded in the timing of the bloom. Over the investigated timeframe, the variations in physical processes due to reduced wind speeds within wind wakes from OWFs resulted in 7 % decrease of total amount of Chl-a across the domain ($Chla_{tot}$). Although $Chla_{tot}$ decreased from March to June, larger decreases occurred during the pre-bloom (−8.55 %) than during the bloom (−2.86 %), and positive and negative variations were

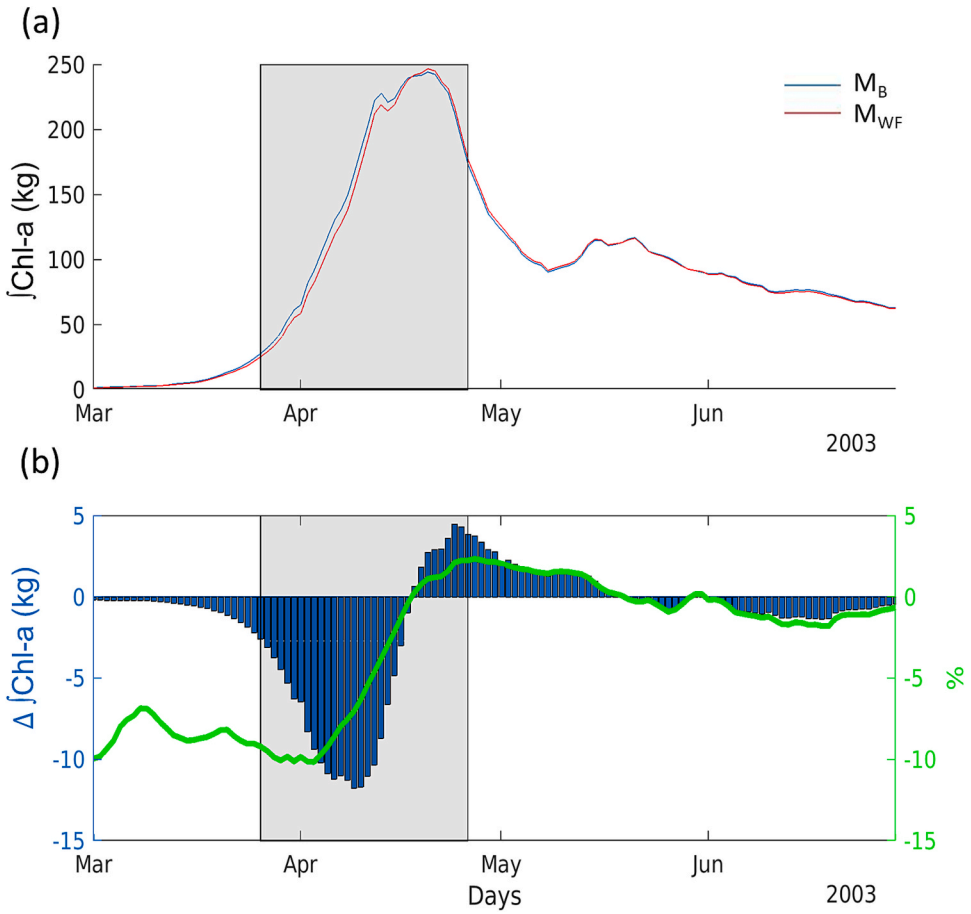

Fig. 3. (a) Time series of daily Chl-a across the entire domain for M_B (blue line) and M_{WF} (red line). (b) Daily absolute values (histogram) and percentages (green line) of the differences (Δ) in $Chla_{tot}$ between M_B and M_{WF}. The grey polygon (a-b) identifies the bloom period. (For interpretation of the references to colour in this figure legend, the reader is referred to the web version of this article.)

counterbalanced during the post-bloom showing an overall small increase (+0.12 %). The highest daily decreases are recorded during the pre-bloom and bloom (Fig. 3b) when the progressive rise in Chl-a is slightly postponed in the M_{WF}. The overall decreases during pre-bloom and bloom periods indicate a progressive reduction in daily Chl-a (Fig. 3 b) across the studied region. Changes in food availability during the bloom can have significant consequences on upper trophic levels, such as zooplankton and fish. For example, *Calanus finmarchicus* is known to sacrifice its egg production when resources are low (Mayor et al., 2009). The reduced concentration of Chl-a during the bloom (Fig. 3) can potentially impact secondary and tertiary grazers (zooplankton and pelagic fish species) over the whole region, while causing them to migrate or becoming more vulnerable to predation at hot-spots with rising production. On the other hand, the limited variation registered during post-bloom is not indicative of minimal effects of OWFs. Although Chl-a remained relatively stable after the bloom, food resources spatially redistributed across the region (Fig. 4) potentially causing different local effects by increasing and decreasing production within different habitats or hydrodynamic regimes. This suggests that the spatial scale plays a crucial role in understanding the effects of OWFs, as focusing solely on temporal scale overlooks potential intrinsic variability that is not captured by temporal averages across space.

3.2. *Physical and biological changes at different phenological stages of the spring bloom*

Addressing the changes caused by operating OWFs at meaningful spatial and temporal scales is crucial to effectively understand OWF-induced impacts. The analyses performed in this study on the modelled outputs have questioned the importance of selecting appropriate temporal and spatial scales for summarising potential changes caused by OWFs, particularly in investigating whether averaging the variables across three phenological periods yields different and unique information. It is important to note that averages may obscure large short-term temporal differences that could be, especially for Chl-a, ecologically significant. Further investigation should take place to represent biological changes at temporal and spatial scales that are ecologically important, especially for targeted analyses such as cumulative ecosystem models or single species models.

Phytoplankton concentration slightly decreased (−7%) in the wind farm scenario at the regional scale (< 240 km north to south). However, examining the spatial distribution of these changes over three periods (Fig. 4) revealed significant spatial variations in Chl-a (Fig. 4 a-c). Local averaged $\Delta\int$Chl-a reached -25 mg m^{-2} during the bloom and $\pm$ 6 mg m^{-2} during post-bloom, showing high variability between the two phenological phases. Before and during the bloom, phytoplankton primarily decreased across the region (Fig. 4 a-b). This is consistent with

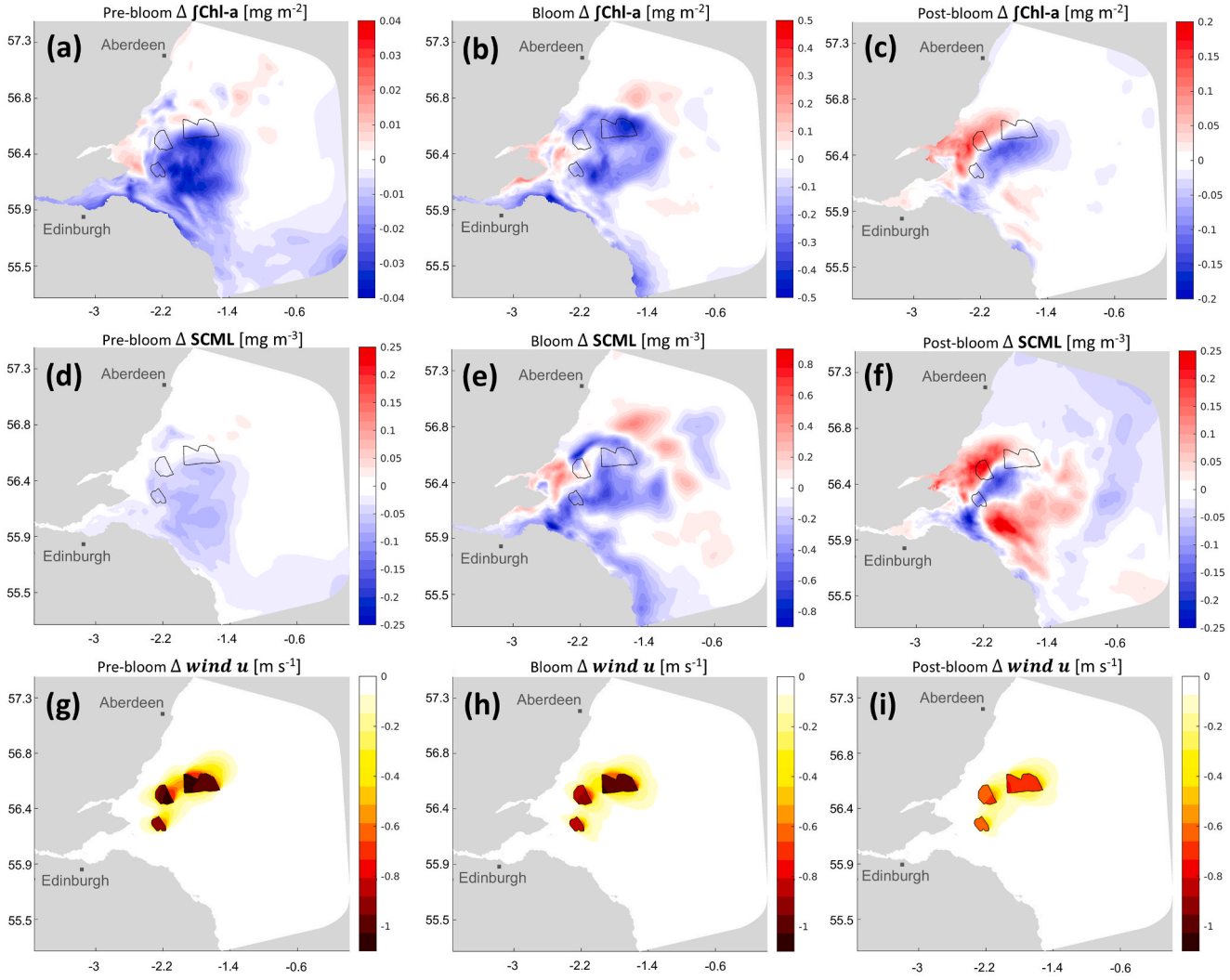

Fig. 4. Maps of variations in depth-integrated Chl-a ($\int$Chl-a) (a-c), subsurface Chl-a maximum layer (SCML (d-f), and wind speed (wind u) (g-i) during pre-bloom, bloom, and post-bloom periods. Black polygon indicates wind farms. Longitude and latitude are reported in the WGS 1984 UTM Zone 30 North coordinate system.

the decreases reported for the entire region (Fig. 3 b). On the other hand, during the post-bloom period, the changes over the entire region (+0.12 %) failed to capture local changes (Fig. 4 c).

The redistribution of Chl-a occurred also at the vertical spatial scale. In the modelled scenario of the Firth of Forth and Tay region, the spatial redistribution of phytoplankton appeared different among phenological periods when considering ∫Chl-a or the subsurface Chl-a maximum layer (SCML) (Fig. 4 a-f). Especially during the post-bloom, the SCMLs increased over regions where ∫Chl-a decreased (Fig. 4 c, f). SCMLs represent hot spot of feeding opportunity for predators, especially during low trophic conditions, when multiple top predators have been linked to forage upon high subsurface Chl-a (Embling et al., 2012; Scott et al., 2010). Although the modelled scenarios showed regions of decreasing ∫Chl-a, local increases at SCML can have ecological effects on the ecosystem by supporting the food patch landscape in less trophic periods such as those during summer. Since SCML rely on upward fluxes of deep nutrient-enriched waters (Cullen, 2015), local increases could be induced by the downwelling and upwelling cells from OWF wakes

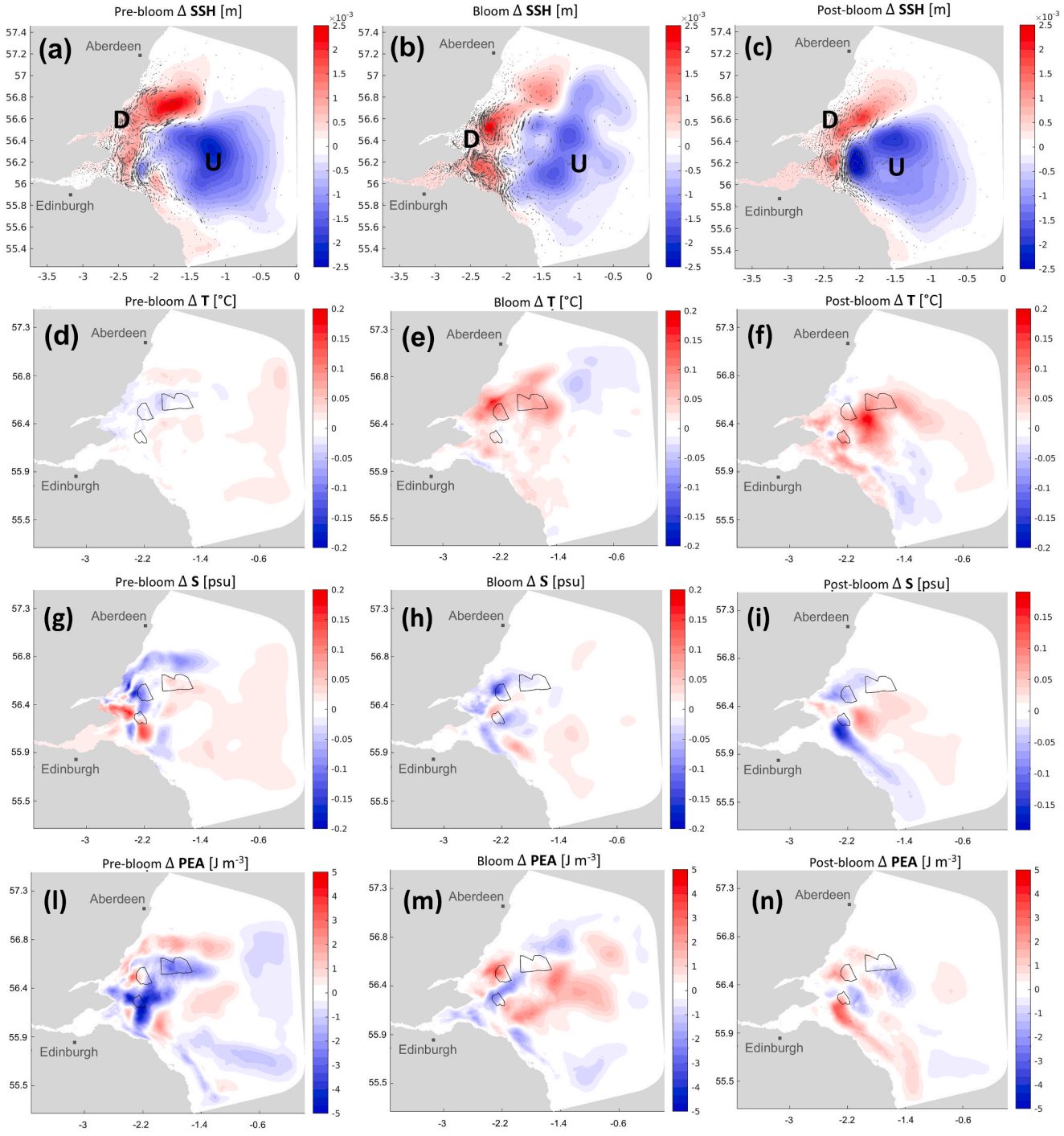

Fig. 5. Maps of variations in sea surface height (SSH) (a-c), depth-averaged temperature (T) (d-f) and salinity (S) (g-i), and potential energy anomaly (PEA) (l-n) during pre-bloom, bloom, and post-bloom periods. Black polygon indicates wind farms. Quiver plots (black) on top of the maps a-c show the resulting horizontal current calculated as the difference between M_{WF} and M_B of u and v components. Downwelling (D – red) and upwelling (U – blue) dipoles are reported on top of the SSH anomaly (Δ). (For interpretation of the references to colour in this figure legend, the reader is referred to the web version of this article.)

(Ludewig, 2015). However, the physical drivers changing Chl-a were difficult to discern from the averaged conditions in the three phenological periods (Fig. 5). Only during the post-bloom, the distribution of ∫Chl-a was correlated to the spatial distribution of the upwelling/downwelling dipole (Fig. 5 c) ($\rho = 0.48$, Table A2 in the Appendix). However, changes in ∫Chl-a were less spatially correlated with the other investigated physical changes across the Firth of Forth and Tay region (Table A2), although physical variations occurred.

Sea surface height (SSH) exhibited a spatially homogeneous effect (Fig. 5 a-c), while changes in PEA, depth-averaged temperature and salinty showed a patchy distribution (Fig. 5 and Fig. A8). Previous modelled studies reported SSH, temperature and salinity changes with the formation of dipoles in the proximity of the wake-impacted area (Broström, 2008; Christiansen et al., 2022a; Floeter et al., 2017; Ludewig, 2015; Paskyabi and Fer, 2012). Dipoles were postulated by Broström (2008) and Ludewig (2015) as one of the main effects of wind speed reduction from offshore wind farms, and their formation can be compared to the effects of wind blowing along a coastline. The difference in SSH (or pressure) due to the reduced Ekman transport results in weak geostrophic current perpendicular to the pressure gradient (from high to low). During the three phenological phases, the Coriolis force deflected the horizontal pressure gradient force, broadly going from west (high pressure) to east (low pressure), into a broadly southward (roughly cyclonic around the upwelling region) steady geostrophic current that is most stable between the upwelling and downwelling sides of the dipole (Fig. 5 a-c) (Broström, 2008; Ludewig, 2015). Perpendicular to the geostrophic current, two relative vortices of opposite signs developed within each upwelling/downwelling region. Similar formations were described in Christiansen et al. (2022) in the central-southern North Sea. The averaged SSH showed that the distribution of dipoles was consistent during the three periods when wind directions were more variable with predominant south-west and north-west wind (Fig. A.7). A similar distribution of SSH appeared in shorter intervals with stable winds from south-west and north-west up to 20-hours (Section 3.3). Since dipoles develops after 10 h of stable wind (Floeter et al., 2022), the predominance of winds from 180°-360° (periods lasting on average 49 ± 67 h) facilitated the distribution of dipoles during the three periods. Other wind directions (from 1° to 180°) lasted for shorter periods (19 ± 27 h) during the simulation. The transient wind events likely caused localised variation in the dipole distribution, which did not manifest in the average distribution of dipoles.

Upwelling and downwelling dipoles are characterised by specific patterns of SSH, temperature and salinity variations (Broström, 2008; Christiansen et al., 2022a; Floeter et al., 2017; Ludewig, 2015; Paskyabi and Fer, 2012), whereas converging SSH results in decreasing salinity and increasing temperature, while diverging SSH on the upwelling region causes increasing salinity and decreasing temperature (Ludewig, 2015), under stratified conditions. The variation in salinity happened to be inversely correlated to PEA and SSH during the three phenological periods ($\rho > -0.5$, except for salinity and SSH during pre-bloom, Table A.2), suggesting that changes in the distribution of stratified waters and dipoles are mainly driven by changes of the salinity gradient. Since wind stress shapes the distribution of river plumes (Clark and Mannino, 2022), the reduced wind speed and altered Ekman transport could redistribute the Forth and Tay plumes, which in turn leads to changes in the stratification of the water column over the region where converging and diverging surface waters developed (dipoles). More details of these processes were examined along transects over shorter periods of time (section 3.3).

3.3. Fine scale changes during prevailing wind conditions

Changes in abiotic variables and Chl-a were averaged over a period of 12 hours after confirming that the established dipoles were stable over time. Shorter periods (4–8 h) would have showed fewer clear dipoles (Fig. A.9 and A.10), and longer period (16–20 h) would have incorporated additional wind directions and tidal phases (ebb-flood), which could have mitigated the OWF effects (Christiansen et al., 2022b). The two 12-hour periods of constant wind direction were selected under similar tidal and wind conditions (see details in Appendix and Fig. A.6).

Changes between M_B and M_{WF} were investigated along a virtual transect crossing Inch Cape OWF to describe i) upwind and downwind (wake lee) conditions under north-west wind (Fig. 6 b) and ii) changes occurring on the left and right sides of the Inch Cape wake under south-west wind (Fig. 6 d).

Dipoles defined by SSH, salinity and temperature were distinguishable at both horizontal (Fig. 6, and Fig. A.13) and vertical scales (Figs. 7, 8). The distribution of dipoles remained similar between periods, though north-west wind produced smaller, patchier, dipoles compared to the formed under south-west wind. These differences could result from the interaction between wind and tidal currents. In this region, the tidal ellipse extends from north-east to south-west (Fig. A.14). When the wind blows from the south-west, aligning with the tidal current direction, dipoles appeared more clearly aligned with the tidal and wind directions, and its impact on absolute values of PEA, horizontal current, temperature and salinity was weaker. During north-west wind, stronger effects on horizontal currents were modelled, which potentially disrupted the formation of large dipoles of SSH, and consequently impacted more temperature, salinity and PEA (Fig. A.13). However, further research is needed to understand the interaction between tides and wind wakes under different wind conditions.

During south-west wind, converging waters (Fig. 6 d) redistributed salinity to the north-east, between OWFs and the coastline, altering temperature and PEA (Fig. A.13). Common effects between the two prevailing winds were identified for sea surface temperatures, which increased by up to 0.4°C during south-west wind and 1°C during north-west wind, both within the wake lee and within Inch Cape. The temperature increases can be attributed to the reduced wind velocities along the wake, which has been described to deform the temperature front (Ludewig, 2015). The increase in sea surface temperatures caused an increase in PEA during the two wind conditions (Figs. 7 and 8).

During north-west wind, a salinity dipole developed with pole centres outside the transect, aligned with the wind wake, where the downwelling pole developed between Inch Cape and Seagreen OWFs (Fig. 6 b). Within the downwind section of the transect (Fig. 7), the salinity dipole develops one after the other by increasing distance from Inch Cape. Increasing temperature and decreasing salinity at the sea surface within the wake lee (30 km from the edge of the farm) showed an expected increase in PEA (+10 J m^{-3}) caused by the reduced surface mixing originating from slower wind speeds along the wake. This area overlapped with increasing SSH, which ultimately defined a weak and small patch of downwelling conditions. The convergence of fresher and warmer waters at the surface enhanced the difference in the gradient of temperature and salinity between surface and bottom, resulting in strengthening of stratification (Fig. 7). The increase of stratification over a region with PEA values between 40 and 60 J m^{-3} persisting over the summer season (seasonally stratified regime) (Fig. 7 h) led to the isolation of surface oligotrophic waters from nutrient-rich deep waters that supports phytoplankton growth (Fig. 7 f). This caused a decrease in subsurface Chl-a along the wake lee over regions of intensified stratification. Conversely, the upwelling throughout most of the water column (characterised by increasing salinity and decreasing temperature beyond 70 km along the transect) reduced stratification (−5 J m^{-3}) over regions of seasonal stratification (Fig. 7 h) causing an increase in Chl-a (+0.4 mg m^{-3}, Fig. 7 f). Hence, the wind speed reduction along the wake generated an opposite effect within and outside the wake lee over similar hydrodynamic conditions (seasonally stratified regimes): Chl-a decreased within the wake in waters with intensified stratification and it increased away from the wake in waters with reduced stratification.

Another increase in Chl-a occurred within Inch Cape, where temperature and salinity decreased (Fig. 7 b,d). This area appeared to be characterised by a potential outflow of colder and fresher waters from

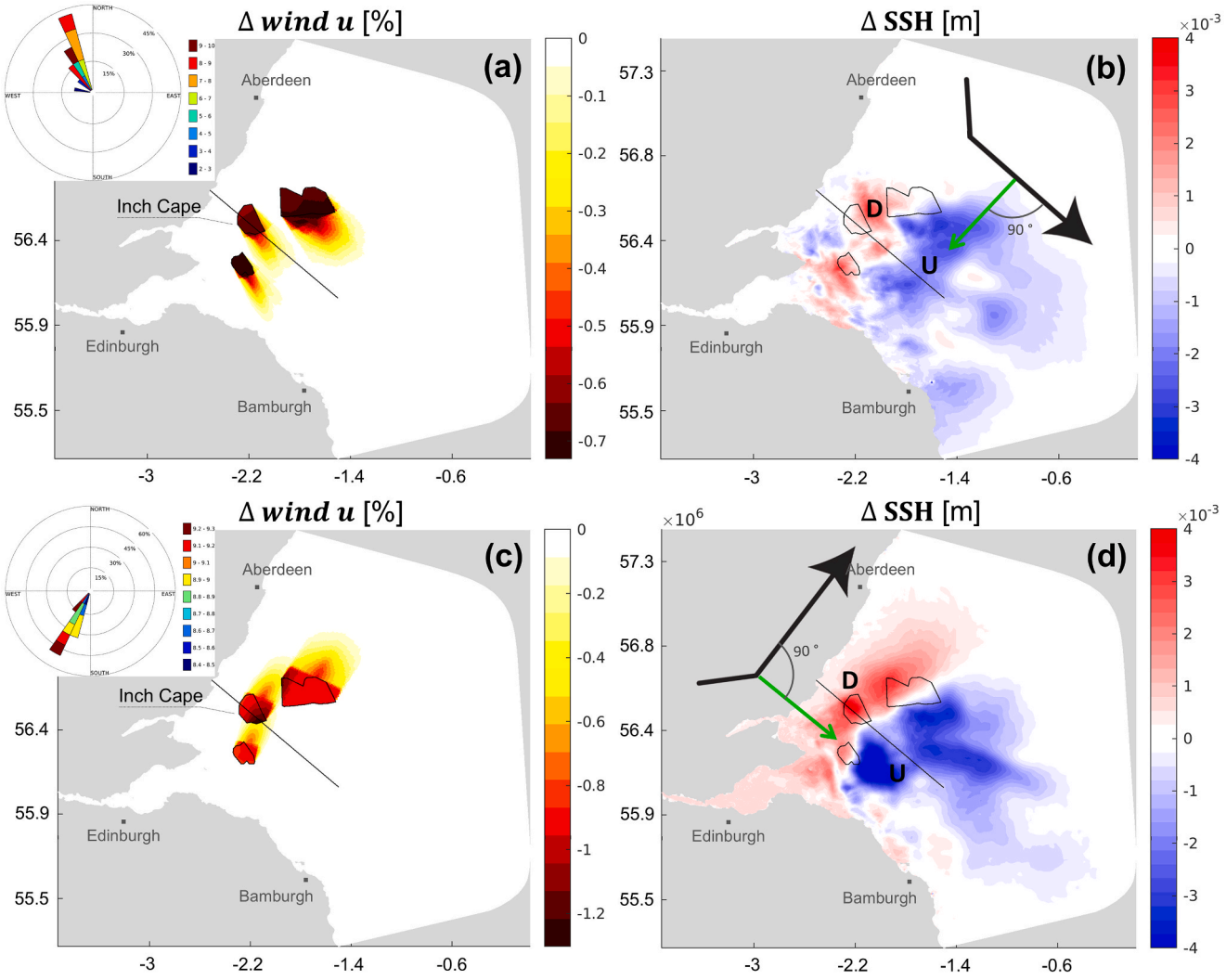

Fig. 6. (a) and (c) show the spatial distribution of parameterised wind speed deficit (%) during 12 h of prevailing wind (wind roses). (b) and (d) show the corresponding changes in sea surface height (SSH) during the two time periods. Upwelling (U) and downwelling (D) regions, the prevailing wind direction (black arrow) and resulting Ekman transport direction (green arrow) are shown in (b) and (d). (For interpretation of the references to colour in this figure legend, the reader is referred to the web version of this article.)

the river Tay, which did not alter stratification (50–60 J m^{-3}) and boosted Chl-a production (+0.6 mg m^{-3}).

During south-west wind conditions (Fig. 6 d, Fig. 8 and Fig. A.13), the reduced surface wind stress and Ekman transport originated a convergence (downwelling) of water masses within the wake to the left of the wake (between Inch Cape and the coastline) and a divergence (upwelling) at the right side of the wake (looking into wind direction) (Ludewig, 2015). Although the selected transect overlaps with the centroid of downwelling at Inch Cape, it captures only a portion of the upwelling region at > 60 km (Fig. 8), whose centre locates on the side of the transect (Fig. 6 d). Along the transect, the upwelling region first appears at the subsurface (10 m at 60–70 km), with decreasing temperature and increasing salinity, and it consequently extends throughout the water column at distances > 70 km from the coastline.

The region adjacent to the coastline exhibited surface Chl-a in permanently mixed and intermittently stratified waters (Fig. 8 e, g) during undisturbed conditions (M_B). Although water masses would depart from the coastline due to Ekman transport, OWFs enhanced the creation of a downwelling region within Inch Cape, where warmer and fresher waters converged mainly at the surface. This led to a greater difference in temperature and salinity between surface and bottom layers, increasing stratification by 7 J m^{-3} (Fig. 8 h). Here, enhanced stratified conditions over permanently mixed and intermittently stratified waters led to increased Chl-a production at the subsurface (0.5 mg m-3, Fig. 8 f at < 30 km along the transect) as nutrients accumulated rather than being flushed away by tidal mixing. Enhanced PEA was identified also during north-west wind in regions of downwelling with converging fresher and warmer waters (Fig. 7), where, instead, caused a decrease in Chl-a over seasonally stratified waters. Therefore, when PEA increased due to converging surface waters induced by OWF wind wakes, it enhanced Chl-a production in areas where the baseline conditions were permanently mixed or intermittently stratified, and Chl-a decreased in seasonally stratified waters.

The right side of the transect (see labels in Fig. 8) exhibited a similar increase in sea surface temperature to those reported by Ludewig (2015), extending up to 30 km from the farm. The whole region exhibiting increased surface temperature was characterised by increased PEA (1 J m^{-3}) and reduced surface Chl-a (−0.5 mg m^{-3}). However, further along the transect, beyond 70 km, an upwelling cell developed, where PEA decreased by 4 J m^{-3} and subsurface Chl-a increased (0.2 mg m^{-3}) in baseline seasonally stratified waters (PEA > 60 m^{-3}) (Fig. 8).

From a general perspective, wind direction influenced the spatial location of dipoles. Phytoplankton production was enhanced by increasing PEA (7 J m^{-3}) in permanently mixed and intermittently

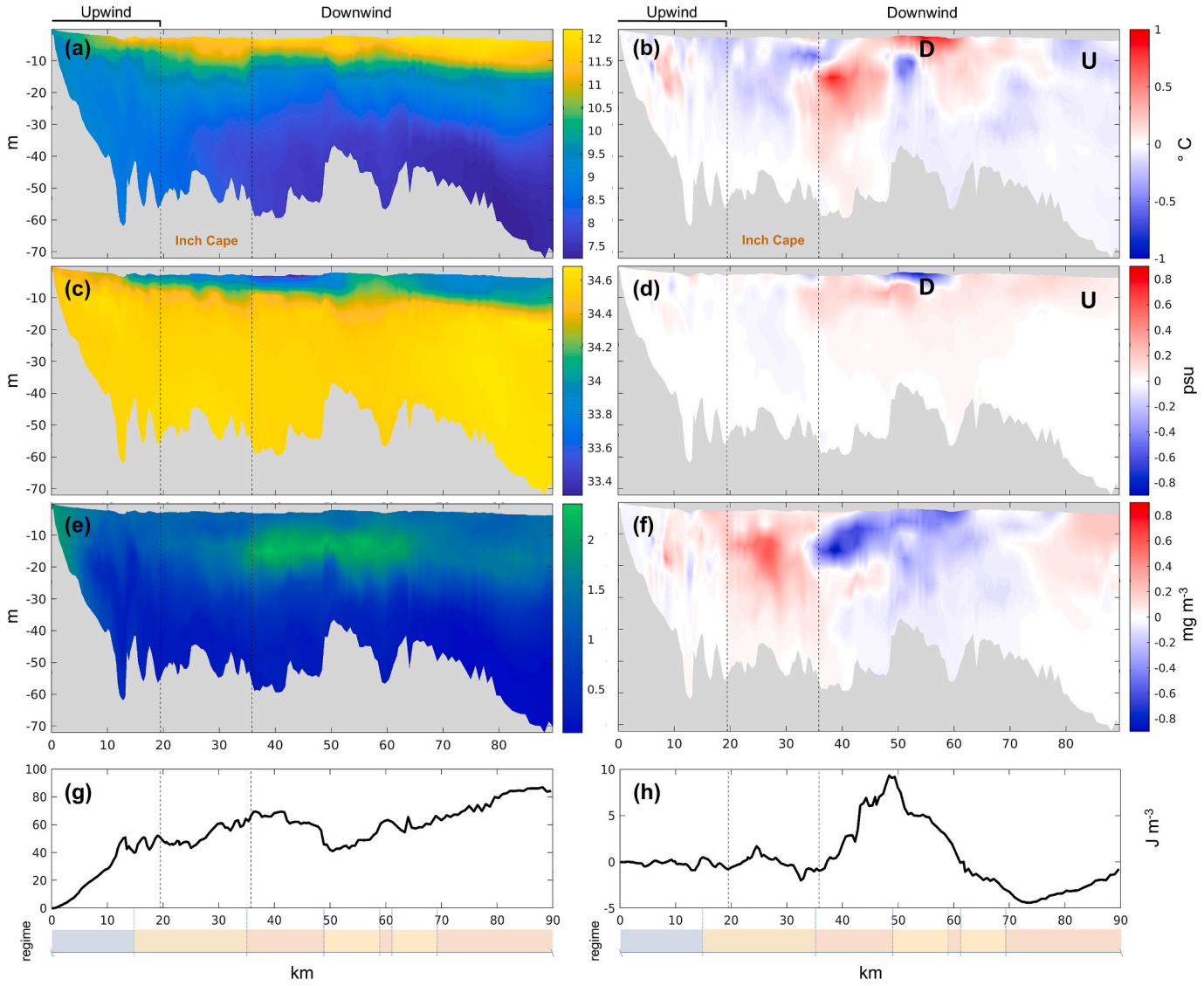

Fig. 7. Transect of temperature, salinity, Chl-a, and PEA for undisturbed conditions (a, c, e) and the anomaly (b, d, f) during prevailing north-west wind. Plots on the left show M_B and those on the right show $\Delta = M_{WF} - M_B$. Vertical dashed lines define the region occupied by Inch Cape farm. Upwelling (U) and downwelling (D) regions are indicated along temperature and salinity transects. Regimes are coloured coded: blue – permanently mixed, yellow – intermittently mixed, orange – seasonally mixed. Modelled data along the transect are available at https://github.com/azampollo/Modelling-OWFs.git. (For interpretation of the references to colour in this figure legend, the reader is referred to the web version of this article.)

stratified waters, while decreasing PEA (4 J m^{-3}) had the opposite effect in seasonally stratified waters. Furthermore, a consistent pattern of increasing sea surface temperature and PEA is found along the wake lee and within downwelling regions, while decreasing PEA is found in upwelling regions. The distribution of dipoles influenced the stratification of the water column by changing salinity and temperature, and ultimately Chl-a. The overlap between downwelling and regions with increasing PEA suggest that the convergence of fresher and warmer waters at the surface (Broström, 2008; Ludewig, 2015) enhanced stratification by increasing the surface to bottom density gradient. In contrast, the diverging surface waters in the upwelling region (Broström, 2008; Ludewig, 2015) weakened stratification.

4. Conclusion

This study, using fine temporal and spatial scale outputs from a validated coupled FVCOM-ERSEM model of the Firth of Forth and Tay region, showed that reduced wind speed from OWF wakes is likely to affect Chl-a concentration both temporally and spatially. Carrying out analysis at a range of ecologically important temporal and spatial scales has highlighted the level of spatial and temporal variability in abiotic variables and Chl-a and the limitations and advantages of averaging across time and (three-dimensional) space.

The effects of OWFs are scale dependent, meaning that their impact on marine ecosystems can vary significantly depending on the spatial and temporal resolution at which observations and analyses are conducted. At broader scales, general trends such as overall reductions in Chl-a appeared limited ($Chla_{tot}$ reduced by 7 %). These summaries can hide localized or short-term variations that may be ecologically significant. For instance, while $Chla_{tot}$ showed minimal change during the post-bloom period, finer-scale assessments can reveal distinct regions of greater increase or decrease, particularly in subsurface layers such as the SCML which may be of particular importance to other ecosystem components. This variability highlights the importance of considering multiple scales to fully understand and predict the influence of OWFs on marine productivity and food web dynamics.

The virtual subsampled transects provided insights into the fine-scale spatial variations of Chl-a. Changes in Chl-a occurred over areas

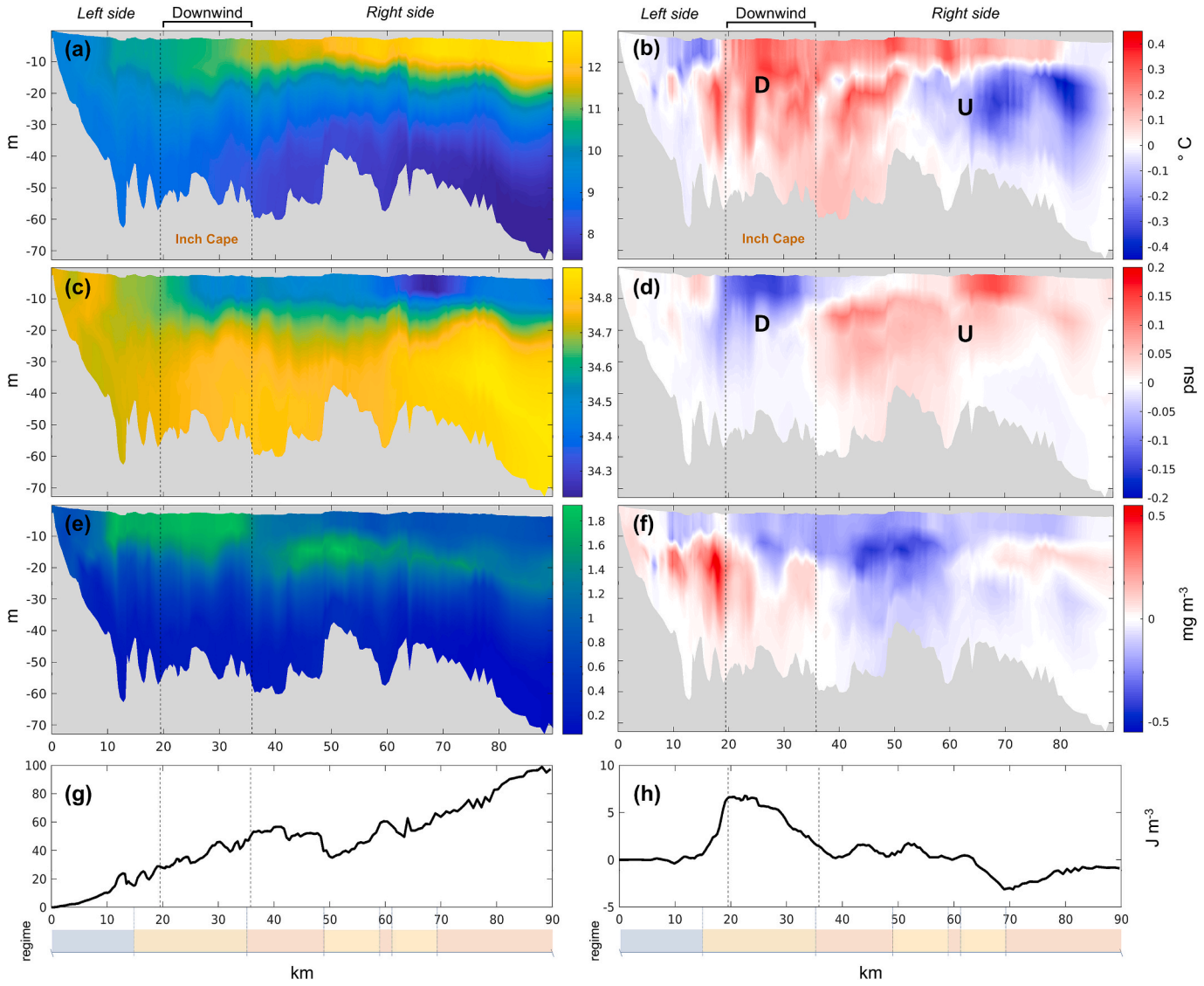

Fig. 8. Transect of temperature, salinity, Chl-a, and PEA for undisturbed conditions (a, c, e) and the anomaly (b, d, f) during prevailing north-west wind. Plots on the left show M_B and those on the right show $\Delta = M_{WF} - M_B$. Vertical dashed lines define the region occupied by Inch Cape farm. Upwelling (U) and downwelling (D) regions are indicated along temperature and salinity transects. Regimes are coloured coded: blue – permanently mixed, yellow – intermittently mixed, orange – seasonally mixed. Modelled data along the transect are available at https://github.com/azampollo/Modelling-OWFs.git. (For interpretation of the references to colour in this figure legend, the reader is referred to the web version of this article.)

influenced by the dipoles, with the effects ultimately coming through the changes in the strength of stratification. More stratified waters developed near downwelling regions, causing a decrease of Chl-a in seasonally stratified waters and an increase of Chl-a in permanently mixed and intermittently stratified waters. In contrast, upwelling in regions with saltier and cooler waters (typically originating to the east of OWFs) caused an overall decrease in stratification and increase in Chl-a. Thus, variations in PEA within upwelling and downwelling areas were associated with changes in Chl-a in seasonally stratified waters.

4.1. *Current limitations and pathways forward*

The potential OWF-induced impacts on the physical and biogeochemical dynamics of shelf seas is complex and dependent on a range of factors, from the turbine types to the environmental conditions, such as hydrodynamic regimes and habitats in which OWFs are situated.

Among the various impact pathways associated with OWFs, the present study focused on a single effect of operational farms: the reduction in wind speed within a fixed distance of 30 km from the farm, measured at 10 m above the sea surface. OWFs are known to induce a broader range of atmospheric and oceanic changes. For instance, wind farms interact differently with the atmosphere depending on meteorological conditions causing variable lengths and intensity of wind wakes. Longer and more persistent wakes have been observed under stable atmospheric conditions, where limited vertical mixing allows the wake effects to extend further downstream (Platis et al., 2018). Additionally, the variability of wind deficit must be considered at different altitudes, as the reduction in wind speed at the hub height (~100 m) can differ from those measured at the sea surface, which has showed not only to decrease but also to locally accelerate (Hasager et al., 2024). These variations in surface wind and turbulence can lead to contrasting oceanographic responses, depending on the prevailing hydrodynamic conditions. For instance, under prolonged stratified conditions, enhanced surface mixing (often driven by increased wind stress) can stimulate phytoplankton growth by allowing deep nutrient-rich waters to reach the surface by either breaking or shoaling/deepening the pycnocline (Carranza et al., 2018). Consistently, our study showed that reduced wind stress at the surface strengthened stratification by

increasing the discrepancy between surface and bottom temperature, which ultimately led to a stronger isolation of subsurface Chl-a within nutrient-depleted waters and its decline in seasonally stratified waters.

In addition to atmospheric effects, turbine foundations (fixed or floating) alter turbulence, currents, bed shear stress and stratification in shelf seas (Austin et al., 2025; Christiansen et al., 2023; Dorrell et al., 2022; Floeter et al., 2017). One of their primary effects is the enhancement of turbulence, which can increase bed shear stress at the scale of the turbine (Austin et al., 2025) and weaken stratification in the water column (Schultze et al., 2020), ultimately changing nutrient resuspension and benthic ecological communities (Damveld et al., 2018). The alteration of benthic communities, along with the introduction of new epistructural biomass, such as the blue mussel (*Mytilus edulis*) colonising turbine foundations (Slavik et al., 2019), is likely to influence nutrient cycling in the vicinity of OWFs. These biological drivers can co-regulate nutrient availability to phytoplankton communities through top-down processes, alongside bottom-up physical processes, potentially reshaping species composition and or the quality of food resources. To capture these dynamics, biogeochemical models such as ERSEM should incorporate top-down regulatory mechanisms of nutrient and foraging pathways introduced by OWF-related processes. Indeed, marine ecosystems may exhibit complex responses to offshore wind farms, and these dynamics should be integrated into future ecosystem models (Isaksson et al., 2023).

Additionally, rising water temperatures and salinity changes driven by climate change (Stocker et al. 2013) can shift the baseline conditions at which the impacts of OWFs are assessed. For instance, seasonally stratified waters may experience intensified stratification under warmer climates, potentially benefitting from the enhanced vertical mixing induced by wind turbine foundations. On the other hand, farm wind wakes were found to be associated with rising sea surface temperatures, which may further intensify stratification in areas not affected by the foundation-induced mixing. As OWFs are built to help mitigate climate change driven by fossil fuel emissions (European Commission, 2020), understanding the effects of large-scale installations in the North Sea is needed as they are likely to change the regional climate (Ze et al., 2024) and oceanography, whose processes are tightly interconnected. A clear example of interconnected feedbacks between atmosphere and the ocean is the influence of wind wakes on ocean waves (van der Molen et al., 2014; Paskyabi and Fer, 2012), and in turn, the impact of sea surface waves on wind energy extraction (Ferčák et al., 2022). Current approaches have so far overlooked these looping interactions due to limitations in modelling resources. To fully evaluate the potential impacts of OWFs in a changing climate, future modelling scenarios require fully coupled frameworks integrating atmospheric, oceanic (hydrodynamics and waves), biogeochemical and ecosystem processes.

The current study applied available methods to predict the potential effects of OWF-induced wakes in shelf seas, aiming to enhance the understanding of a simplified single component within a highly interconnected ocean system. By isolating and examining the influence of a specific factor, such as reduced wind speed within farm wakes, it becomes possible to assess the extent to which phenomena impact ocean dynamics and the individual contribution of this to OWF-induced changes. However, future work should endeavour to fully characterise the complexity of the potential effects as a whole. Overall, the outcomes of this study contribute to building a foundational understanding of the potential impacts of OWFs on marine systems towards the development of more advanced and integrated modelling frameworks.

Funding

This research has been supported by a MarCRF (Marine Collaboration Research Forum, jointly sponsored by the University of Aberdeen and the Scottish Government Marine Directorate) (United Kingdom) PhD grant awarded to Arianna Zampollo. Additional funding was provided by PELAgIO NE/X008835/1 which is part of the 'The Ecological Consequences of Offshore Wind' (ECOWind) programme, funded by the Natural Environment Research Council (NERC) (United Kingdom).

CRediT authorship contribution statement

Arianna Zampollo: Writing – review & editing, Writing – original draft, Validation, Investigation, Formal analysis, Data curation, Conceptualization. **Rory O'Hara Murray:** Writing – review & editing, Validation, Supervision, Software, Methodology, Formal analysis, Conceptualization. **Alejandro Gallego:** Writing – review & editing, Conceptualization. **Beth Scott:** Writing – review & editing, Supervision, Resources, Funding acquisition, Conceptualization.

Declaration of competing interest

The authors declare that they have no known competing financial interests or personal relationships that could have appeared to influence the work reported in this paper.

Acknowledgements

The authors thank the colleagues in the Marine Directorate of the Scottish Government (United Kingdom) and EU Project IMPRESS, for collecting and providing the observational data used to validate aspects of the models, and Dr. Yuri Artioli, Plymouth Marine Laboratory (United Kingdom), for supplying the NEMO-ERSEM AMM7 model outputs.

Appendix A. Supplementary data

Supplementary data to this article can be found online at https://doi.org/10.1016/j.pocean.2025.103512.

References

Akhtar, N., Geyer, B., Rockel, B., Sommer, P.S., Schrum, C., 2021. Accelerating deployment of offshore wind energy alter wind climate and reduce future power generation potentials. Sci. Rep., 11, 11826. https://doi.org/10.1038/s41598-021-91283-3.

Ali, K., Schultz, D.M., Revell, A., Stallard, T., Ouro, P., 2023. Assessment of Five Wind-Farm Parameterizations in the Weather Research and Forecasting Model: A Case Study of Wind Farms in the North Sea. J. Phys.: Conf. Ser. 2767, 092015. https://doi.org/10.1175/MWR-D-23-0006.1.

Arso Civil, M., Quick, N.J., Cheney, B., Pirotta, E., Thompson, P.M., Hammond, P.S., 2019. Changing distribution of the east coast of Scotland bottlenose dolphin population and the challenges of area-based management. Aquat. Conserv. Mar. Freshw. Ecosyst., 29, 178–196. https://doi.org/10.1002/aqc.3102.

Austin, M.J., Unsworth, C.A., Van Landeghem, K.J.J., Lincoln, B.J., 2025. Enhanced bed shear stress and mixing in the tidal wake of an offshore wind turbine monopile. Ocean Sci., 21, 81–91. https://doi.org/10.5194/os-21-81-2025.

Barton, B., De Dominicis, M., O'Hara Murray, R., Campbell, L., 2022. Scottish Shelf Model 3.02 - 27 Year Reanalysis. https://doi.org/10.7489/12423-1.

Benesty, J., Chen, J., Huang, Y., and Cohen, I., 2009. Pearson Correlation Coefficient, in: Noise Reduction in Speech Processing, vol. 2, Springer Berlin Heidelberg, Berlin, Heidelberg, 1–4. https://doi.org/10.1007/978-3-642-00296-0_5.

Bergstad, O.A., Høines, Å.S., Jørgensen, T., 2002. Growth of sandeel, *Ammodytes marinus*, in the northern North Sea and Norwegian coastal waters. Fish. Res., 56, 9–23. https://doi.org/10.1016/S0165-7836(01)00317-4.

Broström, G., 2008. On the influence of large wind farms on the upper ocean circulation. J. Mar. Syst., 74, 585–591. https://doi.org/10.1016/j.jmarsys.2008.05.001.

Butenschön, M., Clark, J., Aldridge, J. N., Allen, J. I., Artioli, Y., Blackford, J., Bruggeman, J., Cazenave, P., Ciavatta, S., Kay, S., Lessin, G., van Leeuwen, S., van der Molen, J., de Mora, L., Polimene, L., Sailley, S., Stephens, N., and Torres, R., 2016. ERSEM 15.06: a generic model for marine biogeochemistry and the ecosystem dynamics of the lower trophic levels, Geosci. Model Dev., 9, 1293–1339. https://doi.org/10.5194/gmd-9-1293-2016.

Carpenter, J.R., Merckelbach, L., Callies, U., Clark, S., Gaslikova, L., Baschek, B., 2016. Potential Impacts of Offshore Wind Farms on North Sea Stratification. PLoS One 11, e0160830. https://doi.org/10.1371/journal.pone.0160830.

Carranza, M.M., Gille, S.T., Franks, P.J.S., Johnson, K.S., Pinkel, R., Girton, J.B., 2018. When Mixed Layers Are Not Mixed. Storm-Driven Mixing and Bio-optical Vertical Gradients in Mixed Layers of the Southern Ocean. J. Geophys. Res. Oceans 123, 7264–7289. https://doi.org/10.1029/2018JC014416.

Carter, M.I.D., Boehme, L., Cronin, M.A., Duck, C.D., Grecian, W.J., Hastie, G.D., Jessopp, M., Matthiopoulos, J., McConnell, B.J., Miller, D.L., Morris, C.D., Moss, S.E. W., Thompson, D., Thompson, P.M., Russell, D.J.F., 2022. Sympatric Seals, Satellite Tracking and Protected Areas: Habitat-Based Distribution Estimates for Conservation

and Management. Front. Mar. Sci., 9, 875869. https://doi.org/10.3389/fmars.2022.875869.
Chen, C., Liu, H., Beardsley, R.C., 2003. An Unstructured Grid, Finite-Volume, Three-Dimensional, Primitive Equations Ocean Model: Application to Coastal Ocean and Estuaries. J. Atmospheric Ocean. Technol., 20, 159–186. https://doi.org/10.1175/1520-0426(2003)020<0159:AUGFVT>2.0.CO;2.
Christiansen, N., Daewel, U., Djath, B., Schrum, C., 2022a. Emergence of Large-Scale Hydrodynamic Structures Due to Atmospheric Offshore Wind Farm Wakes. Front. Mar. Sci., 9, 818501. https://doi.org/10.3389/fmars.2022.818501.
Christiansen, N., Daewel, U., Schrum, C., 2022b. Tidal mitigation of offshore wind wake effects in coastal seas. Front. Mar. Sci., 9. https://doi.org/10.3389/fmars.2022.1006647.
Christiansen, N., Carpenter, J. R., Daewel, U., Suzuki, N., and Schrum, C., 2023. The large-scale impact of anthropogenic mixing by offshore wind turbine foundations in the shallow North Sea, Front. Mar. Sci., 10. https://doi.org/10.3389/fmars.2023.1178330.
European Commission, Offshore renewable energy, 2020. https://energy.ec.europa.eu/topics/renewable-energy/offshore-renewable-energy_en.
Cox, S.L., Embling, C.B., Hosegood, P.J., Votier, S.C., Ingram, S.N., 2018. Oceanographic drivers of marine mammal and seabird habitat-use across shelf-seas: A guide to key features and recommendations for future research and conservation management. Estuar. Coast. Shelf Sci., 212, 294–310. https://doi.org/10.1016/j.ecss.2018.06.022.
Cullen, J.J., 2015. Subsurface Chlorophyll Maximum Layers: Enduring Enigma or Mystery Solved? Annu. Rev. Mar. Sci., 7, 207–239. https://doi.org/10.1146/annurev-marine-010213-135111.
Daewel, U., Akhtar, N., Christiansen, N., Schrum, C., 2022. Offshore wind farms are projected to impact primary production and bottom water deoxygenation in the North Sea. Commun. Earth Environ., 3, 1–8. https://doi.org/10.1038/s43247-022-00625-0.
Damveld, J. H., van der Reijden, K. J., Cheng, C., Koop, L., Haaksma, L. R., Walsh, C. a. J., Soetaert, K., Borsje, B. W., Govers, L. L., Roos, P. C., Olff, H., and Hulscher, S. J. M. H., 2018. Video Transects Reveal That Tidal Sand Waves Affect the Spatial Distribution of Benthic Organisms and Sand Ripples, Geophys. Res. Lett., 45, 11,837-11,846. https://doi.org/10.1029/2018GL079858.
Declerck, M., Trifonova, N., Hartley, J., Scott, B.E., 2023. Cumulative effects of offshore renewables: From pragmatic policies to holistic marine spatial planning tools. Environ. Impact Assess. Rev., 101, 107153. https://doi.org/10.1016/j.eiar.2023.107153.
Dorrell, R. M., Lloyd, C. J., Lincoln, B. J., Rippeth, T. P., Taylor, J. R., Caulfield, C. P., Sharples, J., Polton, J. A., Scannell, B. D., Greaves, D. M., Hall, R. A., and Simpson, J. H., 2022. Anthropogenic Mixing in Seasonally Stratified Shelf Seas by Offshore Wind Farm Infrastructure, Front. Mar. Sci., 9. https://doi.org/10.3389/fmars.2022.830927.
Dunn, R.E., Duckworth, J., Green, J.A., 2023. A framework to unlock marine bird energetics. J. Exp. Biol., 226, jeb246754. https://doi.org/10.1242/jeb.246754.
Edwards, K.P., Barciela, R., Butenschön, M., 2012. Validation of the NEMO-ERSEM operational ecosystem model for the North West European Continental Shelf. Ocean Sci., 8, 983–1000. https://doi.org/10.5194/os-8-983-2012.
Embling, C.B., Illian, J., Armstrong, E., van der Kooij, J., Sharples, J., Camphuysen, K.C. J., Scott, B.E., 2012. Investigating fine-scale spatio-temporal predator–prey patterns in dynamic marine ecosystems: a functional data analysis approach. J. Appl. Ecol., 49, 481–492. https://doi.org/10.1111/j.1365-2664.2012.02114.x.
Emeis, S., 2010. A simple analytical wind park model considering atmospheric stability. Wind Energy 13, 459–469. https://doi.org/10.1002/we.367.
Ferčák, O., Bossuyt, J., Ali, N., Cal, R.B., 2022. Decoupling wind–wave–wake interactions in a fixed-bottom offshore wind turbine. Appl. Energy 309, 118358. https://doi.org/10.1016/j.apenergy.2021.118358.
Floeter, J., van Beusekom, J.E.E., Auch, D., Callies, U., Carpenter, J., Dudeck, T., Eberle, S., Eckhardt, A., Gloe, D., Hänselmann, K., Hufnagl, M., Janßen, S., Lenhart, H., Möller, K.O., North, R.P., Pohlmann, T., Riethmüller, R., Schulz, S., Spreizenbarth, S., Temming, A., Walter, B., Zielinski, O., Möllmann, C., 2017. Pelagic effects of offshore wind farm foundations in the stratified North Sea. Prog. Oceanogr., 156, 154–173. https://doi.org/10.1016/j.pocean.2017.07.003.
Floeter, J., Pohlmann, T., Harmer, A., Möllmann, C., 2022. Chasing the offshore wind farm wind-wake-induced upwelling/downwelling dipole. Front. Mar. Sci., 9. https://doi.org/10.3389/fmars.2022.884943.
Friedland, K.D., Mouw, C.B., Asch, R.G., Ferreira, A.S.A., Henson, S., Hyde, K.J.W., Morse, R.E., Thomas, A.C., Brady, D.C., 2018. Phenology and time series trends of the dominant seasonal phytoplankton bloom across global scales. Glob. Ecol. Biogeogr., 27, 551–569. https://doi.org/10.1111/geb.12717.
Harris, M.P., Bogdanova, M.I., Daunt, F., Wanless, S., 2012. Using GPS technology to assess feeding areas of Atlantic Puffins *Fratercula arctica*. Ringing Migr., 27, 43–49. https://doi.org/10.1080/03078698.2012.691247.
Hasager, C.B., Imber, J., Fischereit, J., Fujita, A., Dimitriadou, K., Badger, M., 2024. Wind Speed-Up in Wind Farm Wakes Quantified From Satellite SAR and Mesoscale Modeling. Wind Energy 27, 1369–1387. https://doi.org/10.1002/we.2943.
Hersbach, H., Bell, B., Berrisford, P., Biavati, G., Horányi, A., Muñoz Sabater, J., Nicolas, J., Peubey, C., Radu, R., Rozum, I., Schepers, D., Simmons, A., Soci, C., Dee, D., Thépaut, J-N., 2023. ERA5 monthly averaged data on pressure levels from 1940 to present. Copernicus Climate Change Service (C3S) Climate Data Store (CDS). https://doi.org/10.24381/cds.6860a573 (Accessed on 13-Feb-2023).
Isaksson, N., Scott, B. E., Hunt, G. L., Benninghaus, E., Declerck, M., Gormley, K., Harris, C., Sjöstrand, S., Trifonova, N. I., Waggitt, J. J., Wihsgott, J. U., Williams, C., Zampollo, A., and Williamson, B. J., 2023. A paradigm for understanding whole ecosystem effects of offshore wind farms in shelf seas, ICES J. Mar. Sci., fsad194. https://doi.org/10.1093/icesjms/fsad194.
Ludewig, E., 2015. On the Effect of Offshore Wind Farms on the Atmosphere and Ocean Dynamics, Springer International Publishing. Cham. https://doi.org/10.1007/978-3-319-08641-5.
Mayor, D.J., Anderson, T.R., Pond, D.W., Irigoien, X., 2009. Egg production and associated losses of carbon, nitrogen and fatty acids from maternal biomass in Calanus finmarchicus before the spring bloom. J. Mar. Syst., 4, 505–510. https://doi.org/10.1016/j.jmarsys.2008.12.019.
O'Hara Murray, R., 2017. Modelling Scottish shelf seas 22.
Paskyabi, M.B., Fer, I., 2012. Upper Ocean Response to Large Wind Farm Effect in the Presence of Surface Gravity Waves. Energy Procedia 24, 245–254. https://doi.org/10.1016/j.egypro.2012.06.106.
Platis, A., Siedersleben, S.K., Bange, J., Lampert, A., Bärfuss, K., Hankers, R., Cañadillas, B., Foreman, R., Schulz-Stellenfleth, J., Djath, B., Neumann, T., Emeis, S., 2018. First in situ evidence of wakes in the far field behind offshore wind farms. Sci. Rep., 8, 2163. https://doi.org/10.1038/s41598-018-20389-y.
Platt, T., Fuentes-Yaco, C., Frank, K.T., 2003. Spring algal bloom and larval fish survival. Nature 423, 398–399. https://doi.org/10.1038/423398b.
Rodionov, S.N., 2004. A sequential algorithm for testing climate regime shifts. Geophys. Res. Lett., 31. https://doi.org/10.1029/2004GL019448.
Room, A.H., Franco-Gaviria, F., Urrego, D., 2022. H.: Rshift STARS Manual - Regime Shift Analysis for Paleoecological Data v2.1, 6.
Schultze, L.K.P., Merckelbach, L.M., Carpenter, J.R., 2020. Storm-induced turbulence alters shelf sea vertical fluxes. Limnol. Oceanogr. Lett., 5, 264–270. https://doi.org/10.1002/lol2.10139.
Scott, B. E., Sharples, J., Wanless, S., Ross, O. N., Frederiksen, M., and Daunt, F., 2006. The use of biologically meaningful oceanographic indices to separate the effects of climate and fisheries on seabird breeding success, in: Top Predators in Marine Ecosystems, edited by: Boyd, I. L. and Wanless, S., Cambridge University Press, 46–62. https://doi.org/10.1017/CBO9780511541964.005.
Scott, B.E., Sharples, J., Ross, O.N., Wang, J., Pierce, G.J., Camphuysen, C.J., 2010. Sub-surface hotspots in shallow seas: fine-scale limited locations of top predator foraging habitat indicated by tidal mixing and sub-surface chlorophyll. Mar. Ecol. Prog. Ser., 408, 207–226. https://doi.org/10.3354/meps08552.
Slavik, K., Lemmen, C., Zhang, W., Kerimoglu, O., Klingbeil, K., Wirtz, K.W., 2019. The large-scale impact of offshore wind farm structures on pelagic primary productivity in the southern North Sea. Hydrobiologia 845, 35–53. https://doi.org/10.1007/s10750-018-3653-5.
Stocker, T. F., Qin, D., Plattner, G. K., Alexander, L. V., Allen, S. K., Bindoff, N. L., ... & Xie, S. P., 2013. Technical summary. In Climate change 2013: the physical science basis. Contribution of Working Group I to the Fifth Assessment Report of the Intergovernmental Panel on Climate Change, 33-115. Cambridge University Press. https://doi.org/10.1017/CBO9781107415324.005.
Taylor, K.E., 2001. Summarizing multiple aspects of model performance in a single diagram. J. Geophys. Res. Atmospheres 106, 7183–7192. https://doi.org/10.1029/2000JD900719.
Trifonova, N.I., Scott, B.E., De Dominicis, M., Waggitt, J.J., Wolf, J., 2021. Bayesian network modelling provides spatial and temporal understanding of ecosystem dynamics within shallow shelf seas. Ecol. Indic., 129, 107997. https://doi.org/10.1016/j.ecolind.2021.107997.
van der Molen, J., Smith, H.C.M., Lepper, P., Limpenny, S., Rees, J., 2014. Predicting the large-scale consequences of offshore wind turbine array development on a North Sea ecosystem. Cont. Shelf Res., 85, 60–72. https://doi.org/10.1016/j.csr.2014.05.018.
van Leeuwen, S., van, Tett, P., Mills, D., and Molen, J. van der, 2015. Stratified and nonstratified areas in the North Sea: Long-term variability and biological and policy implications. J. Geophys. Res. Oceans 120, 4670–4686. https://doi.org/10.1002/2014JC010485.
Vikebø, F.B., Korosov, A., Stenevik, E.K., Husebø, Å., Slotte, A., 2012. Spatio-temporal overlap of hatching in Norwegian spring-spawning herring and the spring phytoplankton bloom at available spawning substrata. ICES J. Mar. Sci., 69, 1298–1302. https://doi.org/10.1093/icesjms/fss083.
Wanless, S., 1998. Summer sandeel consumption by seabirds breeding in the Firth of Forth, south-east Scotland. ICES J. Mar. Sci., 55, 1141–1151. https://doi.org/10.1006/jmsc.1998.0372.
Ze, J., Xiuchun, Y., Ang, C., Dong, Y., Min, Z., Lunda, W., 2024. Localized Eco-climatic impacts of onshore wind farms: a review. J. Resour. Ecol., 15, 151–160. https://doi.org/10.5814/j.issn.1674-764x.2024.01.013.